Figures 5-7 show the solutions of the problem B of the instantaneous energy release $e_0 = 4\pi 25.5$ with simultaneous motion of the heat-removing piston with velocities $\alpha_0 = 1.88$, 2.90, 3.22, and 3.40 (lines 1-4).

As we can see, as the velocity of the piston and, correspondingly, the heat removal on it increase, the velocity of the forward front of the perturbations decreases, and the velocity of the shock wave increases, and therefore the region of heating in front of the shock wave decreases in size. At the same time, the relative change in the velocity of the shock wave is small, while the velocity of the forward front of the perturbation wave is quite substantial.

The closeness of the values of the pressures (the graphs are not shown) directly behind the shock waves deserves special attention.

LITERATURE CITED

1. V. P. Korobeinikov, "Propagation of a strong spherical detonation wave in heat-conducting gas," Dokl. Akad. Nauk SSSR, 113, No. 1 (1957).
2. V. E. Neuvazhaev, "Propagation of a spherical detonation wave in a heat-conducting gas," Prikl. Mat. Mekh., 26, No. 6 (1962).
3. A. A. Samarskii and Yu. P. Popov, Difference Schemes for Gas Dynamics [in Russian], Nauka, Moscow (1975).
4. L. I. Sedov, Similarity Methods and Dimensional Analysis in Mechanics [in Russian], Nauka, Moscow (1965).
5. P. P. Volosevich and E. I. Levanov, Self-Similar Solutions to the Equations of Gas Dynamics Taking into Account Nonlinear Heat Conduction [in Russian], Tbilisi (1977).

MICROMECHANICS OF DYNAMIC DEFORMATION AND FAILURE

A. K. Divakov, L. S. Kokhanchik, Yu. I. Meshcheryakov, and M. M. Myshlyaev

UDC 539.374:620.178.7

As demonstrated in [1-4], dynamic deformation and failure of materials proceeds under conditions of marked distribution for particle velocity. This distribution governs not only the dependence of mechanical properties on deformation rate, but also material spalling resistance. The statistical nature of the occurrence of dynamic deformation and failure processes at the microlevel makes it possible by analogy with liquid and gas mechanics to use as a characteristic of these processes a distribution function for particle velocity which gives complete information about processes at the microlevel. However, for many practical purposes, it is entirely satisfactory to know only the first two features, i.e., average particle velocity and particle velocity dispersion. As will be shown below, these two characteristics may be determined simultaneously during a single act of shock loading for a specimen.

A study of material ductility and strength is often carried out on the basis of analyzing time profiles for loading and unloading waves, a record of which is accomplished by means of various types of fast-acting sensors, i.e., manganin, piezoceramic, variable capacitance etc. Laser interferometers occupy a special place among this type of recorder, making it possible to measure local dynamic movements and the free surface velocity of specimens. One of the main virtues of interferometers is their sensitivity to particle velocity distribution. Use of laser interferometry makes it possible not only to record the time profile of a shock wave, but also to obtain quantitative information about the evolution of the particle velocity distribution function at loading and unloading fronts. This information is particularly valuable in combination with microstructural studies of materials, since it makes it possible to study structural changes in the material during dynamic deformation. Whereas the time profile for the shock wave characterizes dynamic deformation and failure processes at the microlevel, the velocity distribution function and its features are microscopic characteristics of these processes.

Leningrad. Translated from Zhurnal Prikladnoi Mekhaniki i Tekhnicheskoi Fiziki, No. 3, pp. 135-144, May-June, 1987. Original article submitted March 3, 1986.

The present work is devoted to an experimental study of the spalling failure of aluminum A-998 and aluminum alloy D16 in the microsecond range of loading duration. Specimen loading under uniaxial deformation conditions was accomplished by means of a pneumatic impact machine in the velocity range 100-300 m/sec with a compression pulse duration at the top of the plateau of 0.5-1.0 μsec and a maximum pressure up to 3 GPa. Recording of the time profiles for free surface velocity of the target was accomplished by means of a laser differential interferometer (LDI), and simultaneously with the interferogram a record was made of the intensity of laser radiation reflected from the free surface of the target. For this purpose part of the reflected radiation was fed to a separate photorecorder. In all of the tests the radiation intensity remained constant over the whole period of pulse recording.

The majority of specimens subjected to shock loading were then studied by optical or scanning microscopy. Determination of the amount of particle velocity dispersion was accomplished from interferograms for free surface velocity. This is based on using the contrast of the interference picture of pulses, by which we understand the ratio of actually observed interference signal pulse amplitude to that which would occur in the absence of particle velocity distribution. As follows from analyzing the operation of LDI carried out in [5], interference picture contrast is connected with the particle velocity distribution function by the relationship

$$I = \int_{-\infty}^{\infty} f(v - v_0) \cos k(v - v_0)\, dv, \tag{1}$$

where v_0 is average particle velocity in the loading or unloading waves; $f(v - v_0)$ is a particle velocity distribution function; I is contrast of the interference picture. If it is assumed that the distribution function has a Gaussian form

$$f(v - v_0) = \frac{1}{\sqrt{2\pi}\,\Delta v} \exp\left[-\frac{(v - v_0)^2}{2(\Delta v)^2}\right], \tag{2}$$

where Δv is particle velocity dispersion, then contrast and dispersion are connected by a simple relationship obtained by substituting (1) in (2):

$$I = \exp\left[-\frac{k^2(\Delta v)^2}{4}\right]. \tag{3}$$

Whence it is possible to calculate Δv with contrast of the interference signal known from the experiment.

The analysis of LDI operation carried out in [5] is only valid for comparatively small (~10% of the average particle velocity) dispersion values. As experiments indicate, a reduction in interference signal amplitude only occurs to a certain threshold dispersion value, after which there is a sharp break in pulses of the interference picture, which appears as a reduction in the number of pulses of the interference signal with simultaneous restoration of the initial pulse amplitude, i.e., contrast of the interference picture. A quantitative correlation of dispersion with the number of pulses may be established on the basis of the following analysis of LDI operation. The latter may be presented as two interacting point intercoherent sources S_1 and S_2, one of which radiates a direct beam, and the second is delayed in time $\tau_d = S_1S_2/c$ (c is velocity of light). The LDI scheme and its representation in the form of two sources is shown in Figs. 1 and 2. In accordance with interferometry principles, at each point of maximum exposure waves arrive from sources S_1 and S_2 in phase, which means that for each point at the surface of maximum exposure the condition

$$|\mathbf{r}_1 - \mathbf{r}_2| = m\lambda_0, \quad m = 1, 2, 3, \ldots, \tag{4}$$

is fulfilled, where $\mathbf{r}_1$ and $\mathbf{r}_2$ are radius-vectors from S_1 and S_2 to an arbitrary point of the surface of maximum exposure. The number of surfaces of maximum exposure

$$N = 2S_1S_2/\lambda. \tag{5}$$

Here λ is wavelength of laser radiation reflected from a moving target. If the target is still, then

$$N_0 = 2S_1S_2/\lambda_0, \tag{6}$$

where λ_0 is wavelength of laser radiation used in the LDI scheme. If some point of space is fixed, and observation is made of the number of surfaces of maximum exposure passing through this point due a change in λ as a result of a Doppler shift in frequency, we obtain the number of pulses at the LDI output. This determines the difference between the number of maximum exposure surfaces when the target moves (5) and when it is still (6):

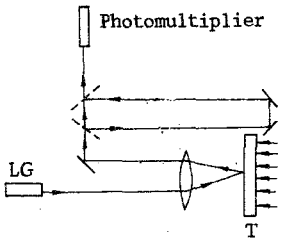

Fig. 1

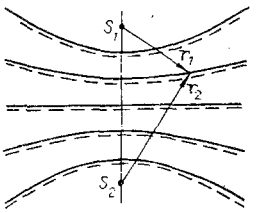

Fig. 2

$$n = \frac{1}{2}(N - N_0) = S_1 S_2 \left(\frac{1}{\lambda} - \frac{1}{\lambda_0}\right). \tag{7}$$

On the other hand the correlation between λ and λ_0 with reflection of a beam from a moving surface is determined by the Doppler effect

$$\lambda \cong \lambda_0 \frac{1}{\left(1 - \frac{2v}{c}\right)}. \tag{8}$$

By substituting (8) in (7) we obtain an equation connecting the number of interference signal pulses with the movement velocity of a target free surface:

$$n = 2\tau_d v/\lambda_0. \tag{9}$$

In fact, it conforms with a similar relationship obtained in [6] for the case when particle velocity distribution is not considered.

Now let sources S_1 and S_2 radiate light whose wavelength varies randomly in the range $\Delta\lambda = \lambda_{max} - \lambda_{min}$. Applied to LDI this means that direct and delayed beams are reflected from the free surface of the target whose individual particles have a velocity scatter within the range $\Delta v = v_{max} - v_{min}$. Each of the beams may be represented in the form of an assembly of elementary beams reacting with specific particles of the target free surface. As a result of interaction and in view of the fact that particles of the free surface have different velocities, elementary beams take on a different value of Doppler shift in frequency, which leads to a reduction in the level of monochromatism for both the direct and delayed beam, i.e., to expansion of the spectrum. This radiation may be represented as irradiation from a point source whose wavelength varies randomly over the recording time in the range $\Delta\lambda = \lambda_{max} - \lambda_{min}$.

Interference of direct and delayed beams at the upper boundary of the spectrum λ_{max} leads to formation of the picture of maximum exposure surfaces, conditionally shown in Fig. 2 by solid lines, and at the lower boundary of the spectrum λ_{min}, by broken lines. It is natural that in view of relationship (4) with $\lambda_{max} \neq \lambda_{min}$ the spatial position of these surfaces does not coincide. An increase in the range $\Delta\lambda$ leads first to deformation of the picture of surface location with a corresponding deterioration in the contrast of the interference signal, and then to an intermittent change in their number. The change in the number of maximum exposure surfaces is determined by the expression [7]

$$\Delta N = \frac{2S_1 S_2 (\lambda_{max} - \lambda_{min})}{\lambda_{max}\lambda_{min}} \cong \frac{2S_1 S_2 \Delta\lambda}{\bar{\lambda}^2}, \tag{10}$$

where $\bar{\lambda}$ is average wavelength of the laser radiation spectrum after reflection from a moving surface. If the velocity of the surface probed by a laser is in the range $\Delta v = v_{max} - v_{min}$, then from expressions (5)-(10) it is easy to obtain the change in the number of pulses at the LDI output as a consequence of particle velocity distribution:

$$\Delta n = 2\tau_d \Delta v/\lambda. \tag{11}$$

The analysis given above indicates that in using this property of the interferometric method as sensitivity to particle velocity distribution, it is possible to measure simultaneously two characteristics of the deformation process, i.e., average particle velocity and particle velocity dispersion. The latter is connected with structural micromechanics of dynamic deformation, and therefore comparison of data for the change in particle ve-

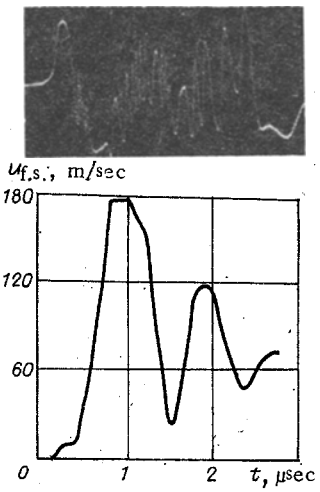

Fig. 3

locity dispersion with metallographic studies of deformed specimens gives additional information about processes at the microlevel. In the present work these studies were carried out on the same specimens for which particle velocity dispersion was determined. With this aim, specimens after testing were cut along one plane in the direction of wave propagation and after polishing and etching they were studied in optical and scanning microscopes. In those specimens where there is separation of a spalled platelet, end and side surfaces of the spalling were also considered. Studies showed that there is a certain conformity between the nature of spalling failure of specimens and the form of interferograms.

For aluminum A-998 a complete record of interferograms and conformity of velocity values obtained on the basis of interpreting pulse pictures and the flight velocity of the striker is typical. Since in all tests the striker was made of the same material as the target, its velocity equalled the maximum value of free surface velocity at the plateau of the pulse. In aluminum A-998 in the loading velocity range being considered there was no disruption for pulses of the interference signal. However, at both the leading and trailing front of the compression pulse the signal amplitude of pulses is markedly below the tuning amplitude, i.e., that which is realized in the absence of particle velocity distribution. Since as was noted above the intensity of laser radiation reflected from the target does not vary, the reduction in pulse amplitude occurs as a result of expansion of the radiation spectrum reflected from the target due to particle velocity distribution. At the same time, in view of the fact that the number of pulses does not vary, and only their amplitude changes, this distribution is not so large that there is disruption of the interference signal for pulses.

A typical interferogram for a compression pulse in aluminum A-998 is shown in Fig. 3. It corresponds to a compression pulse with a free surface velocity at the plateau ~178 m/sec and spalling velocity ~163 m/sec. With a value of the delay arm of the interferometer $\tau_d = 11.7$ nsec, these data relate to 6.5 pulses in the leading and six pulses in the trailing fronts of the pulse, which is also observed in the interferogram. The contrast of the pulse signal in the leading front is 0.07 and in the rear it is 0.42. Then according to expression (3) at the leading front of the pulse $\Delta v = 14$ m/sec, and at the trailing front $\Delta v = 8$ m/sec.

Particle velocity distribution measured by means of an interferometer is a result of the fact that during dynamic deformation neighboring areas of the material move with different velocity, sliding relative to each other. A result of sliding is formation of a chain of micropores orientated along the direction of wave propagation. The region between the chains is free from micropores and other defects.

A fractogram of a transverse section of an aluminum A-998 specimen is shown in Fig. 4a where the average distance between neighboring micropore chains is ~10 μm, which is much less than the average grain size for this material (1-3 mm). Also seen in Fig. 4b together with chains of micropores are areas of a spalling crack formed as a result of the interaction of direct and reflected pressure pulses from the free surface. At a magnification of ×1000 the zig-zag nature of spalling crack geometry is clearly observed. Individual rectilinear sections of the spalling crack are oriented at an angle of 45° to the direction of wave propagation in the specimen, and chains of micropores pass precisely through the point of spalling crack breakage. All of these factors indicate that dynamic deformation of aluminum A-998 proceeds in such a way that the material moves in the form of more or less independent microflows along the direction of wave propagation, and each microflow has its own mass velocity of particles.

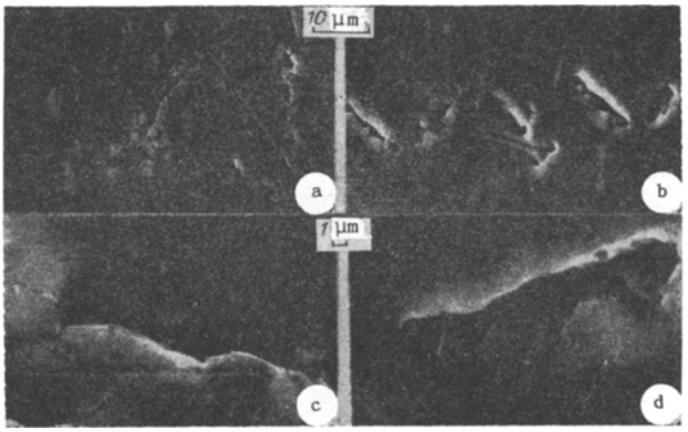

Fig. 4

As can be seen from fractograms, the nature of flow within each of the microflows bounded by lines of deformation and microprobe chains is very uniform. The broken nature of the spalling crack makes it possible to assume that spalling failure in each of the microflows occurs independently of each other along planes of maximum tangential stress. Since the mass velocities of particles in different microflows is not the same, the distance from the free surface at which spalling occurs in each of the microflows is different. The small width of the spalling crack itself (~1 μm, Fig. 4c) and the normal crack geometry in areas of breakage indicates material deformation by slip of the dislocation type within each microflow, although the microflows themselves slide relative to each other in a "viscous" manner.

According to Fig. 4b the spatial scatter of spalling cracks in neighboring flows is on average ~10 μm. With a prolonged compression pulse of ~1 μsec the scatter in microflow velocity is ~10 m/sec, which agrees with estimates carried out above on the basis of measuring the contrast of an interference picture.

In aluminum A-998 the grain size is much greater than the diameter of the interferometer laser beam focused by a lens at the free surface of the target, so that individual grains represent a greater area in relation to the incident beam. This means that the interferometric data obtained in testing aluminum A-998 corresponds to dynamic processes in single crystals forming grains. On the other hand, the diameter of the laser beam may be greater than the distance between deformation lines and micropore chains in crystals (~10 μm), so that during probing of grain boundaries by a laser beam ~10^2 microflows are covered emerging at its surface. Thus, the interference picture obtained with probing of A-998 aluminum specimens reflects the statistical nature of dynamic deformation for an individual material grain. Movement of microflows within grains is a new, larger scale level of dynamic deformation compared with dislocations.

In tests for dynamic deformation of aluminum A-998 it is also noted that grains emerging at the free target surface may be rotated as a whole in relation to the incident beam. As a result of this the interference picture disappears temporarily in the duration period of the leading front of the compression pulse, reappearing after the end of the upper plateau of the pulse. In contrast to this with oblique impact of the target, restoration of the interference picture does not occur during pulse recording. Interferograms of pulses for target free surface velocity for grain rotation (a) and for oblique impact (b) are presented in Fig. 5. On the basis of these data it is possible to conclude that in shock-deformed aluminum A-998 there is grain reorientation which may be considered as a third scale level of dynamic deformation.

Combined analysis of an interference picture of pulses and electron microscope data for studying the failure surface in alloy D-16 leads to different quantitative and qualitative results. Here particle velocity distribution is so broad that there is a jumpwise reduction in the number of pulses of the interference signal compared with that which would occur in the absence of distribution. A typical interferogram demonstrating the disruption of pulses at the leading front of a compression pulse in D-16 is shown in Fig. 6a. The amplitude of the pulse signal is equal to the tuning amplitude only at the very start of the pulse (section AB in Fig. 6b). In section BC due to increasing particle velocity distribution the amplitude of the pulse signal decreases at first, then at point C with a free surface velocity of ~140 m/sec there is disruption of pulses. With the delay arm of the interferometer equal to 224 cm (this relates to 84.5 m/sec for one pulse) the maximum value of velocity in the pulse plateau of 206 m/sec should correspond to 2.4 pulses. Besides this, in the interferogram shown there are only 1.2 pulses. According to expression (11) the reduction observed in the number of pulses ($\Delta n = 1.2$)

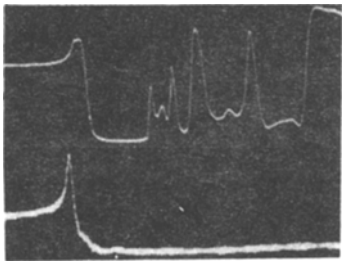

Fig. 5

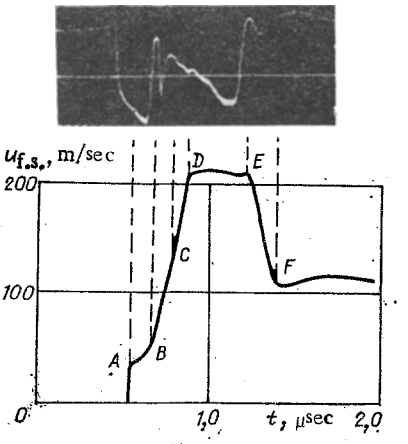

Fig. 6

relates to the dispersion of particle velocity $\Delta v = 102$ m/sec, which is an order of magnitude greater than in aluminum A-998.

We compare the interferometric data obtained with the results of metallographic studies. In specimens of alloy D-16 loaded in the prethreshold region when disruption of pulses of the interference signal has not yet set in, the picture of a transverse section of specimens also contains deformation lines and micropore chains standing at a distance from each other of ~10 μm and oriented along the wave propagation direction, i.e., similar to that which is observed within individual crystals with dynamic deformation of aluminum A-998. On loading D-16 specimens above the critical velocity with which there is disruption of pulses, the picture of a transverse section is complicated by the appearance of thicker bands of micropore chains separated from each other at a distance of 30-40 μm. Since grain size in the test specimens of alloy D-16 is also equal to 30-40 μm, it is possible to confirm that disruption of the interference picture and development of thicker deformation bands and micropore chains at the next scale level is connected with grain boundary sliding in the direction of wave propagation. This slip is accomplished in a viscous way, which is indicated by the nature of the pitted structure of the spalled surface of alloy D-16 specimens, one fractogram of which is presented in Fig. 7a. Attention is drawn to the two typical sizes of pitted structure, i.e., coarse pits of diameter 30-40 μm and finer pits 1-3 μm in diameter surrounding them.

A similar picture with spalling failure for aluminum alloy V-95 was observed by the authors of [8]. They indicated that fine pits have an elliptical shape, and the large axis of the ellipse is directed along the tangent to the circumference of large pits. This points to the shear nature of failure and the possibility of material rotation around the centers of large pits. Our studies also indicate the possibility of this process during spalling failure of alloy D-16 since the shape and size of pits seen in Fig. 7a are similar to those described in [8]. In addition, attention is drawn to one important detail of the internal structure of pits, i.e., the normal geometry of relief lines in the bottom surface of pits. These relief lines (see area 2 in Fig. 7a) with an average size of ~10 μm are evidently areas of the emergence of microflows within individual crystallites. Since each grain projects as a single-crystal body, relief lines are quite specific and of geometrically normal configuration.

Until stresses are so large that they cause grain boundary sliding, movement of microflows within grains comes second after the dislocation level of deformation. On reaching a critical stress value a third level of dynamic deformation sets in, i.e., intergranular slip. However, in contrast to aluminum A-998, the grain size in alloy D-16 is less by a factor of three to four than the laser beam diameter, so that during probing of a specimen surface 10-15 grains are covered. The distribution of grains in velocity (in fact it causes development of thicker bands of micropore chains and longitudinal cracks in D-16 specimens) covers a wider range of velocities, as a result of which there is disruption of interference signal pulses.

It is noted that a spalling crack in alloy D-16 specimens is a randomly oriented wandering line with average spatial scatter of its individual sections in relation to the free surface up to 80-100 μm. With a compression pulse lasting 1 μsec this corresponds to scatter in velocity $\Delta v = 80$-100 m/sec, which coincides very accurately with estimates for dispersion of velocity carried out above on the basis of interferometric data. Analysis of fractograms of the spalled surfaces of alloy D-16 specimens indicates that failure of alloy D-16 proceeds in a ductile fashion, and in contrast to aluminum A-998 separation of third level microflows is accomplished as a result of sliding along the planes of maximum tangential stresses for each of the flows, and as a

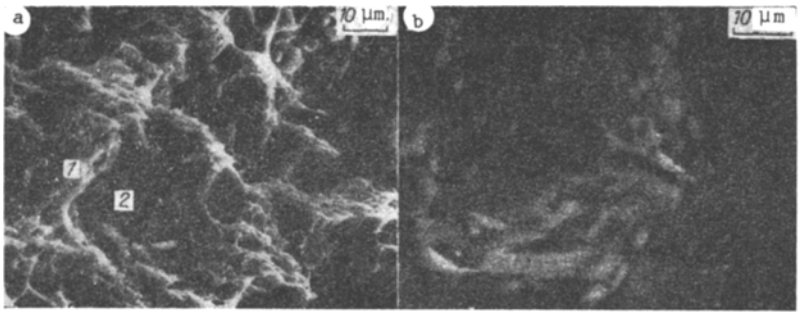

Fig. 7

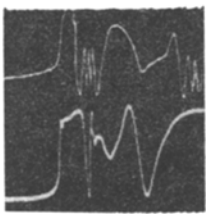

Fig. 8

result of combined effect of separation and shear with simultaneous rotation of microflow as a whole. Studies also show that material rotation is possible not only around the microflow axis, but also in a perpendicular plane. Traces of similar rotation are visible in a fractogram taken from a transverse section of the target (see Fig. 7b). The diameter of the whirl formed by micropores coincides with the distance between longitudinal chains of micropores. This makes it possible to assume that whirl formation is due to the difference in microflow velocities to the right and left of the whirl, i.e., as a result of microflow velocity distribution.

Plastic strain inhomogeneity at the microlevel, as a result of which there is distribution of material particle velocity in loading waves, may be caused both by the nature of the production process (as for alloy D-16 which has an initially fibrous structure in the bar drawing direction), and the dynamic deformation process itself for an initially homogeneous material. This last case is illustrated by interferograms shown in Fig. 8. The upper interferogram was obtained for an annealed specimen of aluminum A-998 with a loading rate of 120 m/sec, and the lower was obtained as a result of repeated loading of the specimen with a rate of ~180 m/sec. Whereas in the upper interferogram there is clear definition of all of the pulses of the interference signal at the leading and trailing fronts of the pulse, in the lower interferogram instead of four pulses (with $v_u = 41$ m/sec for each pulse) there is only one, i.e., there was a jumpwise reduction in the number of pulses as a result of particle velocity distribution. A study of the structure of a transverse section for this target showed the presence of micropore chains oriented along the direction of wave propagation, whereas in the original material these chains were not observed. It is possible to assume that conditions for their formation occurred after the first loading, which created microinhomogeneity for the material structure.

Thus, due to the combined use of an interferometric method for measuring free surface velocity for shock-loaded targets and microstructural analysis of specimens, it is recorded in the present work that dynamic deformation and failure processes at the microlevel are closely connected with nonuniformity of material movement at the microlevel independent of how the inhomogeneity was caused: prior deformation prehistory or material properties. It may be hoped that the movement of a deformed material observed in the form of dynamic microflows will make it possible to develop more realistic criteria for dynamic failure and particularly spalling, which might be based not only on measuring average particle velocities or average stresses, but in the second feature, functions of particle velocity distribution: dispersion of particle velocity in the loading wave.

LITERATURE CITED

1. A. K. Divakov, Yu. I. Meshcheryakov, and L. P. Fadienko, "Particle velocity distribution in the elastic precursor of a compression wave in aluminum," Zh. Tekh. Fiz., 53, No. 10 (1983).
2. A. K. Divakov, Yu. I. Meshcheryakov, and L. P. Fadienko, "Kinetic effects of high-speed deformation of aluminum," Zh. Prikl. Mekh. Tekh. Fiz., No. 1 (1984).
3. Yu. I. Meshcheryakov and A. K. Divakov, "Dispersion of particle velocity in a loading wave and the spalling resistance of aluminum," Zh. Tekh. Fiz., 55, No. 3 (1985).
4. V. A. Likhachev, Yu. I. Meshcheryakov, et al., "Structural levels of deformation and failure with dynamic loading," Izv. Vyssh. Uchebn. Zaved., Fiz., No. 6 (1984).
5. F. R. Asay and L. M. Barker, "Interferometric measurements of shock-induced internal particle velocity and spatial variation of particle velocity," J. Appl. Phys., 45, No. 16 (1974).
6. L. M. Barker, Behavior of Dense Media under High Dynamic Pressure, Gordon and Breach, N. Y. (1968).
7. Yu. V. Baiborodin, L. Z. Kriksunov, and O. N. Litvinenko, Handbook for Laser Technology [in Russian], Tekhnika, Kiev (1978).
8. V. I. Romanchenko, O. I. Marusii, and I. V. Kramarenko, "Microstructure of an aluminum alloy in the early stages of spalling," Probl. Prochn., No. 9 (1983).